Anion Effects in Organic Dye-Sensitized Mesoscopic Solar Cells with Ionic Liquid Electrolytes: Tetracyanoborate vs Dicyanamide

Difei Zhou,[†,‡] Yu Bai,[†,‡] Jing Zhang,[†] Ning Cai,[†,‡] Mei Su,[†,‡] Yinghui Wang,[†] Min Zhang,[†] and Peng Wang*,[†]

State Key Laboratory of Polymer Physics and Chemistry, Changchun Institute of Applied Chemistry, Chinese Academy of Sciences, Changchun 130022, China, and Graduate School, Chinese Academy of Sciences, Beijing 100039, China

Received: October 12, 2010; Revised Manuscript Received: November 25, 2010

We compare the impacts of tetracyanoborate and dicyanamide anions in solvent-free ionic liquid electrolytes upon the optoelectronic features of dye-sensitized solar cells based on an organic push−pull chromophore. With respect to dicyanamide, tetracyanoborate confers a bathochromic and higher photocurrent response upon a dye-coated mesoporous titania film. Numerical simulations on electrical impedance spectroscopies disclose that tetracyanoborate anions evoke a downward displacement of the conduction-band edge of an electrolyte-sinking nanocrystalline film in comparison with dicyanamide, generating a more favorable energy-offset at the titania/dye interface and therefore a better exciton dissociation yield, as proved via the transient emission measurements. An effective recombination reaction rate constant U_{0k} is used to depict the charge-transfer behavior at the titania/electrolyte interface in dye-sensitized solar cells. The negative impact of an about 4 times larger U_{0k} of the dicyanamide cell is overwhelmed by the noticeably higher conduction band edge, leading to the experimentally observed anion-dependent open-circuit photovoltage.

1. Introduction

During the foregone two decades, the dye-sensitized solar cell (DSC) technology[1] has been under active scientific and industrial investigations in virtue of its giant potential as a low-cost photovoltaic device for the sustainable energy supply in the future.[2] In a high-efficiency DSC, ultrafast charge separation at the energy-offset dye/titania interface arises upon absorption of photons with organic chromophores grafted on the interior wall of the titania nanopores. Subsequently, photoinduced electrons traverse through a micrometer-thick nanocrystalline film and come to a current collector, before the occurrence of charge recombination with oxidized dye molecules or triiodide ions in a redox electrolyte. Several critical processes of DSCs toward power generation all take place at the nanocrystal/dye/electrolyte interface, which forms one of extensive research focuses nowadays in this field.

Smart material innovation and systematic device engineering have consecutively impelled the technological advancement of DSCs. To date, a validated efficiency of 11.1% has been achieved by employing a ruthenium polypyridyl complex in conjunction with an acetonitrile-based electrolyte.[3] With regard to the limited resource of ruthenium, metal-free organic dyes have attracted considerable research efforts in past years on account of their superior flexibility of molecular tailoring.[4−9] Moreover, the encapsulation of volatile organic solvents constitutes a major concern on the long-term stable operation of DSCs. In this context, ionic liquid composed of only ions while being liquid at room temperature has emerged as a promising candidate to address this issue, mainly owing to the desirable feature of a negligible vapor pressure.[10,11]

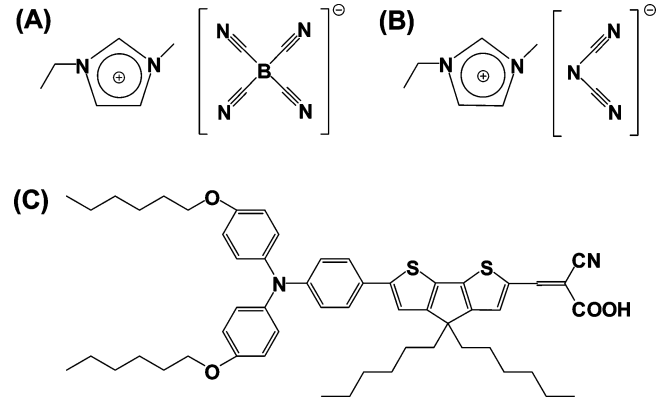

Figure 1. Structures of (A) EMITCB, (B) EMIDCA, and (C) C218.

However, none of ionic liquids featuring a high fluidity like the normal electrolyte solvents such as acetonitrile and 3-methoxypropionitrile has been reported so far. If one considers the most efficient iodide/triiodide redox couple in DSCs, the situation becomes even worse because iodide ions are highly polarizable and could not form ionic liquids with any cations to attain an ambient viscosity lower than 400 cP.[12] Thereby iodide salts are normally mixed with a relatively low-viscosity noniodide ionic liquid to formulate a solvent-free electrolyte in efficient cells.[13] In our previous work,[14] we have identified the eutectic melt of 1,3-dimethylimidazolium iodide (DMII) and 1-ethyl-3-methylimidazolium iodide (EMII) as the most conductive iodide salt, with a melting point lower than 50 °C. On the other hand, either 1-ethyl-3-methylimidazolium tetracyanoborate[15] (EMITCB, Figure 1A) or 1-ethyl-3-methylimidazolium dicyanamide[16] (EMIDCA, Figure 1B) has been widely recognized as a high-conductivity ionic liquid with a dynamic viscosity lower than 25 cP at room temperature. In this contribution, we will construct two ternary ionic liquid elec-

* To whom correspondence should be addressed. E-mail: peng.wang@ciac.jl.cn.
† Changchun Institute of Applied Chemistry.
‡ Graduate School.

10.1021/jp109803n
Published on Web 12/15/2010

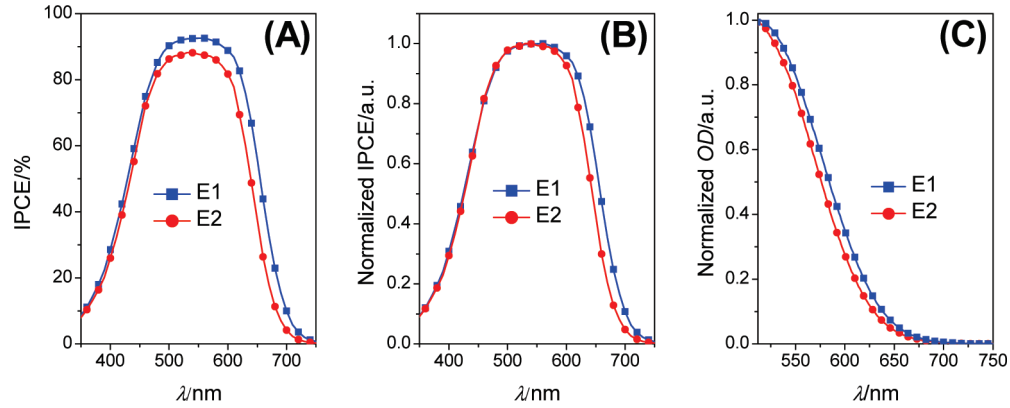

Figure 2. (A) Photocurrent action spectra and (B) plots of normalized IPCE versus wavelength for cells made from electrolytes E1 and E2. An antireflection film was adhered to the testing cell during measurement. Cells were tested using a metal mask with an aperture area of 0.158 cm^2. Film thickness: 7 + 5 μm. (C) Normalized absorptions of C218-coated titania films in contact with E1 and E2. Film thickness: 7 μm. E1, DMII/EMII/EMITCB/I_2/TBP (12/12/16/1.67/3.33, molar ratio); E2, DMII/EMII/EMIDCA/I_2/TBP (12/12/16/1.67/3.33, molar ratio).

trolytes composed of DMII, EMII, and EMITCB (or EMIDCA) and take a close look at the profound impacts of anions on photocurrent action spectra and current density−voltage ($J-V$) characteristics of organic DSCs. Our preliminary experiments have shown that the anion effects reported here are very general for couples of organic push−pull chromophores with a triphenylamine donor and a cyanoacrylic acid acceptor. Thus, the C218 dye (Figure 1C) used as a model photosensitizer in our group is of choice here for systematic studies. The intrinsic origins of some distinguishable photovoltaic features will be further scrutinized by measuring transient emission and absorption as well as electrical impedance spectroscopies.

2. Results and Discussion

The incident photon-to-collected electron conversion efficiency (IPCE) of DSCs represents an accumulative contribution of several critical photophysical and electrical processes, i.e., light-harvesting of the dye-coated titania film, net charge generation at the dye/nanocrystal interface, and carrier collection by the mesoporous semiconducting electrode. Therefore, we first measured the photocurrent action spectra of cells made from electrolytes E1 and E2 to roughly evaluate the anion effects of solvent-free ionic liquids, as illustrated in Figure 2A. The electrolyte composition of E1 is DMII/EMII/EMITCB/I_2/TBP at a molar ratio of 12/12/16/1.67/3.33 and that of E2 is DMII/EMII/EMIDCA/I_2/TBP at the same molar ratio, where TBP denotes 4-*tert*-butylpyridine. The tetracyanoborate electrolyte E1 endows the C218-coated titania film with a 4% higher IPCE maximum compared to the dicyanamide counterpart. In addition, a red-shifting of the onset wavelength of photocurrent response could be readily perceived for the tetracyanoborate electrolyte by normalizing the IPCEs (Figure 2B). The bathochromic effect of tetracyanoborate with respect to dicyanamide can also be observed by measuring the electronic absorptions (Figure 2C) of the C218-coated titania film submerged in the ionic liquid electrolyte E1 or E2.

To figure out the intrinsic origins of their IPCE height difference, we first investigate the kinetic branch ratios depicting the competition between the charge recombination of dye cations with injected electrons and the interception of dye cations by iodide, which could profoundly influence the IPCE maximum.[17−20] The dual-channel charge-transfer kinetics of oxidized dye molecules (D^+) were measured via the laser-induced transient absorption technique with a monochromatic probe light at 782 nm, where the oxidized state rather than the ground state of C218 has a strong absorption.

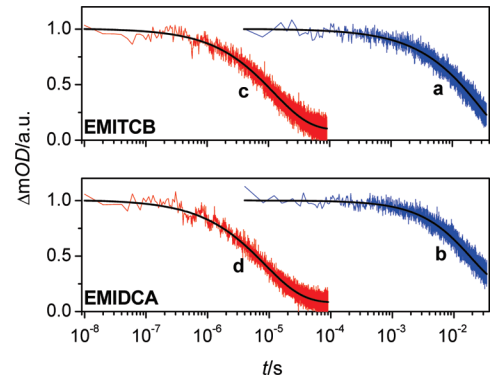

Figure 3. Transient absorption kinetics of a 12-μm thick, C218-coated titania film immersed in inert and electroactive electrolytes. (a) EMITCB/TBP (40/3.33, molar ratio); (b) EMIDCA/TBP (40/3.33, molar ratio); (c) DMII/EMII/EMITCB/I_2/TBP (12/12/16/1.67/3.33, molar ratio); (d) DMII/EMII/EMIDCA/I_2/TBP (12/12/16/1.67/3.33, molar ratio). Absorbance changes (ΔmOD) were measured at a probe wavelength of 782 nm upon pulsed laser excitation. The pulse fluence and excitation wavelength: (a) 55 μJ cm^{-2} at 658 nm; (b) 57 μJ cm^{-2} at 628 nm; (c) 53 μJ cm^{-2} at 655 nm; and (d) 55 μJ cm^{-2} at 636 nm. Smooth black lines are stretched exponential fittings over experimental data obtained by averaging 1000 laser shots.

Excitation fluences were carefully controlled in our kinetic measurements to ensure that ~8.4 × 10^{13} photons cm^{-2} (~0.8 photon per nanoparticle) were absorbed by the dye-coated titania film during every laser pulse. As depicted in Figure 3, the absorption signals could be well fitted to a stretched exponential decay function ($\Delta mOD \propto \exp[-(t/\tau)^{\alpha}]$) to afford the half-reaction times ($t_{1/2}$). In the presence of inert electrolytes where electroactive iodide anions have been removed, the absorption decays (a and b) could be readily attributed to the charge recombination between dye cations and titania electrons. The half-reaction times are 14 and 18 ms for inert electrolytes based on tetracyanoborate and dicyanamide, respectively. However, upon the utilization of electrolytes E1 and E2, the absorption decays are significantly accelerated (c and d), yielding the corresponding $t_{1/2}$ of 9.1 and 6.2 μs. The derived kinetic branch ratios are over 1500 for both cases, indicating that almost 100% of the dye cations can be intercepted by the electron-donating iodide anions. Thereby, we conclude that the difference in the dual-channel charge transfer kinetic competition of dye cations does not make a meaningful contribution to the observed IPCE height variation.

We further resorted to the time-correlated single photon counting (TCSPC) technique to scrutinize the yield of electron

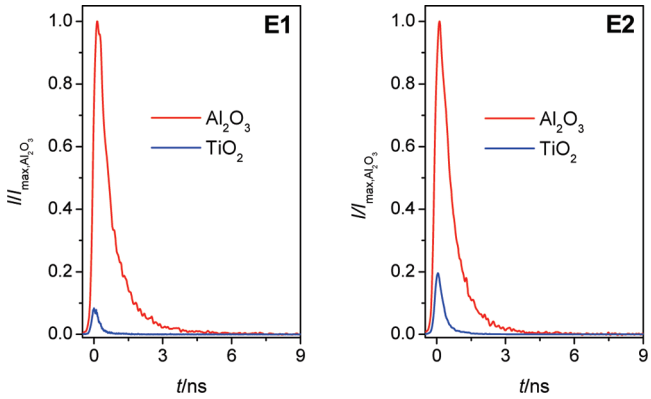

Figure 4. Time-correlated emission decay traces of C218-grafted mesoporous alumina and titania films immersed in electrolytes E1 and E2. Excitation wavelength: 639 nm. Detection wavelength at the wavelength of maximum emission intensity: E1/Al_2O_3, 679 nm; E1/TiO_2, 710 nm; E2/Al_2O_3, 680 nm; E2/TiO_2, 720 nm. The emission intensity (I) was corrected in terms of the film absorbance at 639 nm and further normalized with respect to the emission maximum of a dye-coated alumina film ($I_{max,alumina}$).

injection at the dye/titania interface.[21,22] Reference cells constructed with the C218 dye-coated nanoporous alumina film in contact with electrolytes E1 and E2 feature a strong emission upon laser excitation at 639 nm, as shown in Figure 4. Owing to the lack of an energy offset in favor of charge transfer at the dye/Al_2O_3 interface, the red decay traces can be ascribed to the irradiative and nonirradiative deactivation of excited-state dye molecules. However, the utilization of mesoporous titania film significantly reduces the photoluminescence intensity (I), suggesting the occurrence of electron injection as an alternative nonirradiative channel for deactivation of the excited-state dye molecules. Calculation with the integral of the area under the emission trace on titania and that of alumina affords an electron injection efficiency (η_{inj}) of 96% for the cell made from the tetracyanoborate electrolyte. In contrast, the replacement of tetracyanoborate with dicyanamide leads to a perceivable diminishment of η_{inj}, being 89%. Obviously, a lower exciton dissociation yield in the case of E2 relative to E1 plays a decisive role in the inferior IPCE maximum as shown in Figure 2A.

To estimate the energetics lying behind the kinetics of exciton dissociation, electrical impedance measurements were carried out to derive the conduction band edge (E_c) as well as the distribution of interband states. The E_c of a mesoporous titania electrode correlates with the electron quasi-Fermi level ($E_{F,n}$) and the free carrier density (n) through the following formula

$$E_c = E_{F,n} - k_B T \ln \frac{n}{N_c} \quad (1)$$

where k_B and T refer to the Boltzmann constant and absolute temperature. N_c denotes the density of states in the conduction band. Consider the definition for electron transport resistance (R_t) of a nanoporous semiconducting film[23]

$$R_t = \frac{d}{A_s(1-P)en\mu_0} \quad (2)$$

wherein d, A_s, and P denote the film thickness, area, and porosity, respectively. e is the elementary charge, and μ_0 is the electron mobility and is taken as a constant here to facilitate a comparative study. Moreover, R_t can be determined through

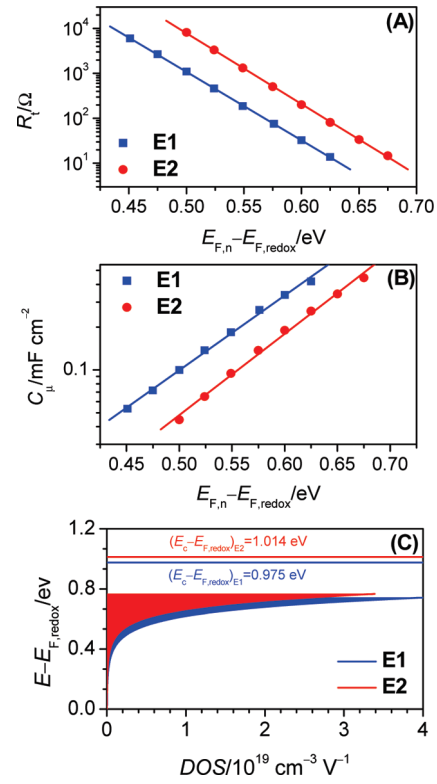

Figure 5. Plots of (A) electron transport resistance (R_t) and (B) chemical capacitance of the titania film. The dotted data are derived from electrical impedance spectroscopies and the solid lines are fittings to eqs 4 and 5. (C) Distribution of density of states (DOS) of cells with electrolytes E1 and E2. The conduction band edges (E_c) relative to $E_{F,redox}$ are also marked out.

numerical modeling of the electrical impedance spectra with the transmission line model proposed by Bisquert et al.[24−26] Integrating eqs 1 and 2 gives

$$R_t = \frac{d}{A_s(1-P)e\mu_0 N_c} \exp\left(\frac{E_c - E_{F,redox}}{k_B T}\right) \exp\left(-\frac{eV}{k_B T}\right) \quad (3)$$

where $E_{F,redox}$ is the Fermi level of a redox electrolyte and the applied potential bias V equals $(E_{F,n}-E_{F,redox})/e$. We remark that from eq 3 one shall expect an exponential dependence of R_t on V with an exponential factor of $-e/k_BT$ (-38.9 V^{-1}). However, this is not manifested in our practical data fittings, which produce exponential factors of -35.1 and -36.3 V^{-1} for cells with E1 and E2, respectively. Hereby, an empirical factor β is introduced to correct this discrepancy, leading to

$$R_t = \frac{d}{A_s(1-p)e\mu_0 N_c} \exp\left(\beta\frac{E_c - E_{F,redox}}{k_B T}\right) \exp\left(-\beta\frac{eV}{k_B T}\right) \quad (4)$$

Note that the potential bias applied here virtually represents the titania Fermi level, in consideration that our impedance measurements were carried out under the open-circuit condition, which essentially guarantees a negligible potential drop in the cell. As shown in Figure 5A, fittings on R_t in terms of eq 4 afford the values of E_c relative to $E_{F,redox}$, being 0.975 and 1.014 eV for the C218-coated titania films in contact with electrolytes E1 and E2, respectively (Table 1). We suspect that the 39 meV

TABLE 1: Parameters Fitted from the R_t, C_μ, and R_{ct}

electrolyte	$E_c - E_{F,redox}$ (eV)	T_c (K)	γ	U_{0k} (10^{21} cm^{-3} s^{-1})
E1	0.975	957	0.63	9.5
E2	1.014	880	0.71	39

upward E_c displacement of the E2 cell relative to that of E1 could stem from the anion-correlated dipole effects upon adsorption onto the titania surface. Further density functional theory (DFT) calculations afforded the dipole moment (μ_D) of the tetracyanoborate anion, which is highly symmetric, to be zero, while the μ_D of dicyanamide reaches ~0.5 D. Additional quantum calculations revealed that the nitrogen atom of the cyano groups on the dicyanamide anion virtually carries more negative charge than the central nitrogen, thus is more favorable for adsorption on titania, as illustrated in Figure 6. A dipole pointing from electrolyte toward titania tends to prompt a conduction band edge elevation,[27] thus explaining the relatively higher E_c position of titania in contact with dicyanamide-containing electrolyte than the tetracyanoborate counterpart.

Apparently, the presence of dicyanamide results in a less favorable thermodynamical driving force for electron injection compared to that of tetracyanoborate. In addition, we note that apart from the E_c displacement, the dissimilar surface states distribution below the conduction band edge may also affect the electron injection yield. The chemical capacitance (C_μ) of a titania/electrolyte interface, which is closely related to the distribution of localized surface states in titania, can also be numerically determined from electrical impedance spectroscopies. The dependence of C_μ on $E_{F,n}$ can be stated as[28]

$$C_\mu = e^2 \frac{N_t}{k_B T_c} \exp\left(\frac{E_{F,redox} - E_c}{k_B T_c}\right) \exp\left(\frac{E_{F,n} - E_{F,redox}}{k_B T_c}\right) \quad (5)$$

where N_t is the density of localized states in the bandgap, and T_c is a characteristic temperature that describes the width of surface state distribution. The larger the T_c is, the wider the distribution of surface states will be. Also note that $(E_{F,n} - E_{F,redox})/e$ virtually equals the V_{oc} of a DSC. Fittings on the chemical capacitance data presented in Figure 5B affords a larger T_c of 957 K for the C218-coated titania film in contact with E1 than that of 880 K for E2. It seems that in comparison with dicyanamide, the tetracyanoborate anions not only prompt a lower E_c but also evokes more surface states at a given Fermi level, which could be qualitatively illustrated by Figure 5C. We suspect that more electron-accepting surface states may partially benefit the electron injection.

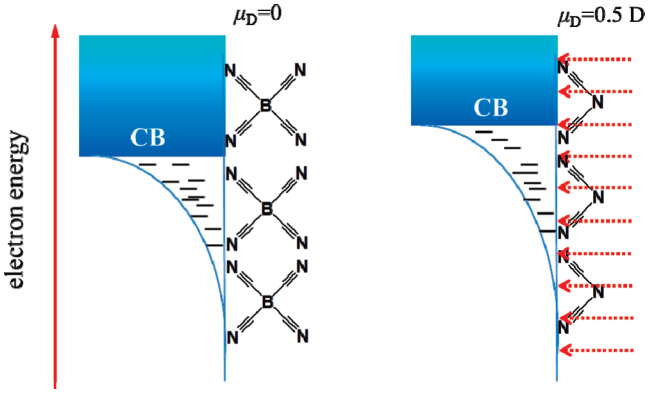

Figure 6. Schematic presentation of the diploe effect on the conduction band edge. The dipole moments (μ_D) of tetracyanoborate and dicyanamide anions have also been marked out. The red arrows indicate the dipole direction.

We further evaluate the photovoltaic parameters of cells made from electrolytes E1 and E2 by recording their $J-V$ characteristics (Figure 7A) under an irradiation of simulated AM1.5G full sunlight, and the photovoltaic parameters are collected in Table 2. The cell with electrolyte E1 displays an open-circuit photovoltage (V_{oc}) of 743 mV, which is evidently incremented to 767 mV upon the employment of E2. It can also be noticed that electrolyte E2 endows the cell with a higher fill factor (FF) of 0.79 in contrast to that of 0.77 obtained with E1. Furthermore, the tetracyanoborate electrolyte generates a short-circuit photocurrent density (J_{sc}) of 14.67 mA cm^{-2}, leading to an overall power conversion efficiency (η) of 8.40%. In contrast, a relatively lower J_{sc} of 13.15 mA cm^{-2} with the E2 electrolyte based on dicyanamide adversely impacts the cell efficiency, affording a relatively lower η of 7.95%.

To understand the open-circuit photovoltage variation of cells with electrolytes E1 and E2, we apply here a modified formula to describe the dependence of charge recombination kinetics in V_{oc} under illumination[29]

$$V_{oc} = \frac{nk_B T}{e} \ln\left(\frac{\Phi}{k_1 n_0^{\gamma} [I_3^-]^{\alpha} + k_2 n_0^{\gamma'} [D^+]^{\alpha'}}\right) \quad (6)$$

where Φ is the photocurrent generation rate and n_0 is the electron density in titania under an equilibrium condition. k_1 and k_2 correspondingly represent the reaction rate constants for charge recombination with I_3^- and D^+. γ and γ' refer to the respective reaction order of titania electrons recombining with I_3^- and D^+. α and α' are the reaction orders of I_3^- and D^+, respectively. Equation 6 virtually discloses that the photovoltage intimately correlates with a kinetic balance between the photocurrent generation and the current loss from the dual-channel charge recombination. However, we note that the contribution from the charge recombination between dye cations and electrons in titania can be essentially neglected, in view of the aforementioned transient absorption measurements revealing a highly efficient net charge separation in our cells. This consideration allows us to obtain

$$V_{oc} = \frac{nk_B T}{e} \ln\left(\frac{\Phi}{k_1 n_0^{\gamma} [I_3^-]^{\alpha}}\right) \quad (7)$$

Herein, by defining $k_0 = k_1[I_3^-]^{\alpha}$ and noting that $n_0 = N_c \exp((E_{F,redox} - E_c)/(k_B T))$, we further introduce a recombination factor U_0 with $U_0 = k_0 N_c^{\gamma} \exp(\gamma(E_{F,redox} - E_c)/(k_B T))$. However, U_0 may not serve well in describing the recombination kinetics

TABLE 2: Photovoltaic Parameters Measured at an Irradiation of 100 mW cm^{-2} AM1.5G Sunlight and Characteristic Cell Parameters Obtained by Fitting the $J-V$ Data in Terms of the Shockley Equivalent Circuit

electrolyte	J_{sc} (mA cm^{-2})	V_{oc} (mV)	FF	η (%)	R_s (Ω)	R_{sh} (Ω)	I_s (A)	I_{ph} (A)
E1	14.67	743	0.77	8.44	12	9.5×10^{16}	2.7×10^{-11}	0.0023
E2	13.15	767	0.79	7.95	13	1.0×10^{17}	1.3×10^{-12}	0.0021

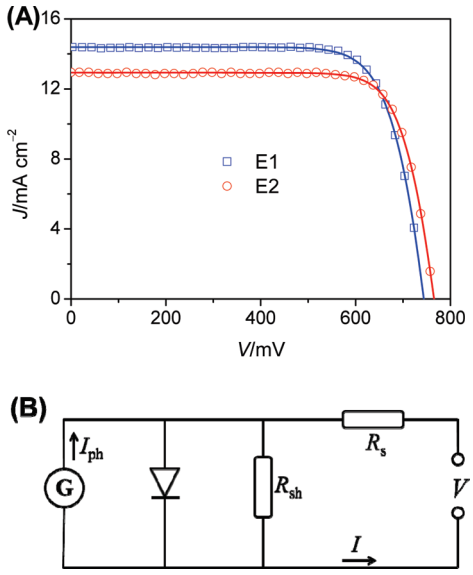

Figure 7. (A) $J-V$ characteristics of cells with electrolytes E1 and E2 measured at an irradiation of 100 mW cm^{-2} AM1.5G sunlight. An antireflection film was adhered to the testing cell during measurement. Cells were tested using a metal mask with an aperture area of 0.158 cm^2. E1, DMII/EMII/EMITCB/I_2/TBP (12/12/16/1.67/3.33, molar ratio); E2, DMII/EMII/EMIDCA/I_2/TBP (12/12/16/1.67/3.33, molar ratio). Film thickness: 7 + 5 μm. The dotted data are experimentally obtained and the solid lines are fittings in terms of eq 12. (B) The Shockley equivalent circuit utilized to simulate the $J-V$ characteristics presented in panel A. The physical meanings of I_{ph}, R_{sh}, and R_s are elucidated in the text.

since that it includes the energetic feature at the titania/dye/electrolyte interface.[30] Thereby, the above expression for U_0 is further expressed as

$$U_0 = U_{0k} \exp \frac{\gamma(E_{F,redox} - E_c)}{k_B T} \quad (8)$$

by referring to an effective reaction rate constant $U_{0k} = k_0 N_c^{\gamma}$, where the thermodynamic information has been subtracted. By noting that the ideality factor $n = 1/\gamma$,[31] combining eqs 7 and 8 leads to

$$V_{oc} = \frac{k_B T}{e\gamma} \ln \frac{\Phi}{U_{0k}} + k_B T \ln \frac{n_0}{N_c} \quad (9)$$

which evaluates the relationship between the interfacial charge recombination kinetics and the V_{oc}. On the other side, it is known that at the open-circuit condition, the photocurrent generation rate is compensated by the recombination rate, i.e., $\Phi = U_n$, eq 7 can be reconstructed as

$$U_n = U_{0k} \exp \frac{\gamma(E_{F,redox} - E_c)}{k_B T} \exp \frac{\gamma V_{oc}}{k_B T} \quad (10)$$

Furthermore, U_n also correlates with the recombination reaction current density j_{rec} through $j_{rec} = edU_n$, while j_{rec} virtually defines the interfacial charge-transfer resistance R_{ct} with $R_{ct} = (1)/(A_s)((\partial j_{rec})/(\partial V_{oc}))^{-1}$,[31] and R_{ct} can be obtained through fitting the impedance spectra with a proper equivalent circuit. Further deduction yields

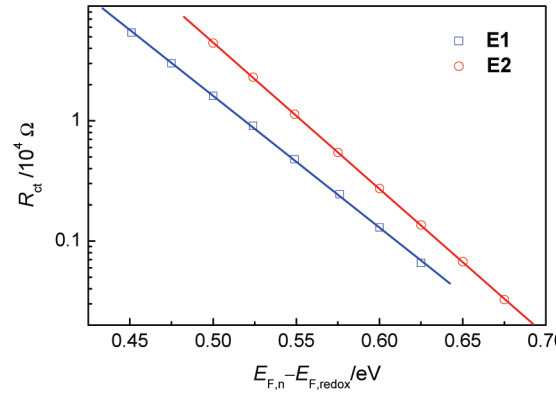

Figure 8. Plots of interfacial charge recombination resistance (R_{ct}) vs the Fermi level difference of the titania film and redox electrolyte. The solid lines are fittings in terms of eq 11.

$$R_{ct} = \frac{k_B T}{e^2 d A_s} (\gamma U_{0k})^{-1} \exp \frac{\gamma(E_c - E_{F,redox})}{k_B T} \exp \frac{-\gamma V_{oc}}{k_B T} \quad (11)$$

As shown in Figure 8, the application of eq 11 to fit R_{ct} affords γ and U_{0k} (Table 1), which exactly constitutes the recombination kinetics at the titania/electrolyte interface. It can be noticed that with respect to the E2 cell, the cell with electrolyte E1 displays a gently smaller reaction order, which is likely related to its relatively wider distribution (larger T_c) of surface states in the bandgap.[31] Moreover, the tetracyanoborate-containing cell features an effective reaction rate constant U_{0k} of 9.5 × 10^{21} cm^{-3} s^{-1}, which is nearly 4 times lower than that of 3.9 × 10^{22} cm^{-3} s^{-1} for the cell made from the dicyanamide counterpart. Thereby, with the aid of eq 10, we can conclude that in comparison with the E1 cell, a 39 mV higher conduction band edge of the cell with electrolyte E2 overwhelmed the adverse effects of faster interfacial charge recombination kinetics (larger U_{0k}) and the gently inferior photocurrent generation (smaller J_{sc}), making a higher open-circuit photovoltage.

In addition to the above discussion, we also applied the Shockley equivalent circuit[29] to simulate the $J-V$ characteristics shown in Figure 7A, taking the reciprocal of the reaction order γ as the ideality factor. Figure 7B presents the equivalent circuit, wherein the series resistance (R_s) accounts for the resistances from the fluorine-doped tin oxide (FTO) substrate and redox electrolyte as well as the charge-transfer resistance on the counter electrode, and the electron transport resistance in titania. The shunt resistance (R_{sh}) is responsible for the current leakage at the FTO/electrolyte contact. The titania/dye/electrolyte interface, which exhibits a diode behavior, has a significant influence on photogenerated current (I_{ph}), reverse saturation current (I_s), and ideality factor (n). By referring to a simulation function depicting the Shockley equivalent circuit and expressed as[32]

$$I = \frac{1}{1 + R_s/R_{sh}} \left\{ I_s \left[\exp \frac{e(V - IR_s)}{nk_B T} - 1 \right] + \frac{V}{R_{sh}} - I_{ph} \right\} \quad (12)$$

Excellent fittings have been obtained as shown by the solid curves in Figure 7A, affording critical characteristic parameters of the cell under AM1.5G full sunlight irradiation (Table 2).

3. Conclusions

In summary, we have investigated the influences of tetracyanoborate and dicyanamide anions, upon the optical and

electrical characteristics of organic DSCs in conjunction with solvent-free ionic liquid electrolytes. In comparison with dicyanamide, tetracyanoborate not only red-shifts the onset wavelength of photocurrent response but also confers a higher IPCE maximum upon a dye-coated mesoporous titania film. Transient emission measurements have disclosed that the employment of tetracyanoborate prompts a better exciton dissociation yield compared to that of dicyanamide. This is further rationalized with a noticeable downward displacement of conduction band edge for the tetracyanoborate cell relative to the dicyanamide counterpart, generating a more favorable energy offset at the titania/dye interface for electron injection. We refer to an effective recombination reaction rate constant U_{0k}, to depict the charge-transfer behavior at the titania/electrolyte interface in dye-sensitized solar cells. The ~4-fold higher U_{0k} of the dicyanamide cell poses an adverse impact on photovoltage, which is however overcompensated by a noticeably higher conduction band edge, explaining the experimentally observed higher open-circuit photovoltage. Our work should shed light on the future interface engineering on more efficient DSCs.

4. Experimental Section

4.1. Materials. Chenodeoxycholic acid (cheno), TBP, and iodine were purchased from Fluka and used without further purification. DMII,[32] EMII,[32] and EMIDCA[16] were prepared according to literature methods. EMITCB and the WERO-2 scattering paste were received as gifts from Dyesol. The synthesis of the C218 sensitizer has been described in our previous paper.[33]

4.2. Cell Fabrication. A double-layer titania film was used as the negative electrode of DSCs. We first deposited a 7-μm-thick transparent layer of 23-nm-sized titania particles via the screen-printing protocol onto a precleaned FTO (Nippon Sheet Glass, Solar, 4 mm thick), and subsequently coated it by a 5-μm-thick second layer of scattering titania particles. A benchtop Ambios XP-1 stylus profilometer was employed to measure the film thickness. The procedures for the synthesis of TiO_2 nanocrystals and the preparation of screen-printing paste were reported previously.[34] A circular TiO_2 electrode (~0.28 cm^2) was stained by immersing it into a dye solution composed of 150 μM C218 and 300 μM cheno in chlorobenzene for 5 h. After washing with acetonitrile and drying by air flow, the dye-coated titania electrode was assembled with a thermally platinized FTO (TEC 15 Ω/□, Libbey-Owens-Ford Industries, 2.2 mm thick) electrode. The electrodes were separated by a 30-μm-thick Bynel (DuPont) hot-melt gasket and sealed up by heating. The internal space was filled with a liquid electrolyte using a vacuum backfilling system. The electrolyte-injecting hole on the counter electrode made with a sand-blasting drill was sealed with a Bynel sheet and a thin glass cover by heating.

4.3. Photovoltaic Measurements. A Keithley 2400 source meter and a Zolix Omni-λ300 monochromator equipped with a 500-W xenon lamp were used for the measurements of photocurrent action spectra, with a wavelength sampling interval of 10 nm and a current sampling time of 2 s under the full computer control. A Hamamatsu S1337−1010BQ silicon diode used for IPCE measurements was calibrated in National Institute of Metrology, China. During the photocurrent action spectrum measurements, a white light-emitting diode was used to bias a testing cell with ~1.0 mA cm^{-2} background current. A model LS1000−4S-AM1.5G-1000-W solar simulator (Solar Light Company, USA) in combination with a metal mesh was employed to give an irradiance of 100 mW cm^{-2}. The light intensity was tested with a PMA2144 pyranometer and a calibrated PMA 2100 dose control system. $J-V$ characteristics were obtained by applying a bias potential to a testing cell and measuring photocurrent with a Keithley 2602 source meter under the full computer control. The measurements were fully automated using Labview 8.0. A metal mask with an aperture area of 0.158 cm^2 was covered on a testing cell during all measurements. An antireflection film (λ < 380 nm, ARKTOP, ASAHI Glass) was adhered to the DSC photoanode during IPCE and $J-V$ measurements. The short-circuit photocurrent densities measured under this solar simulator are well consistent with the integral of IPCEs over the AM1.5G spectrum (ASTM G173−03), within 5% errors.

4.4. Transient Emission and Absorption Measurements. TCSPC measurements were performed on a LifeSpec-II fluorescence spectrometer equipped with an EPL635 laser diode. Transient absorption measurements were carried out with a LP920 laser flash spectrometer in conjunction with a nanosecond tunable OPOLett-355II laser. The sample was kept at a 45° angle to the excitation beam. The probe light from a steady-state xenon arc lamp was passed through various optical elements, samples, and a monochromator before being detected by a fast photomultiplier tube and recorded with a TDS 3012C digital signal analyzer.

4.5. Electrical Impedance Measurements. Electrical impedance experiments were performed under illumination of a white light-emitting diode on an IM6ex electrochemical workstation, with a frequency range from 50 mHz to 100 kHz and a potential modulation of 20 mV. A potential bias was applied to equal the open-circuit photovoltage at a given irradiation intensity, meeting the requirement of zero current. The obtained impedance spectra were fitted with the Z-view software (v2.80, Scribner Associates Inc.).

4.6. Computational Details. The ground-state geometries of tetracyanoborate and dicyanamide were fully optimized without symmetry constraints by the DFT method[36] with hybrid Beck's three-parameter functional and Lee−Yang−Parr functional (B3LYP).[37,38] The 6-31G(d,p) basis set was used for all atoms. All calculations reported here were performed with the Gaussian09 program package.[39]

Acknowledgment. The National 973 Program (No. 2007-CB936702 and No. 2011CBA00702), the National Science Foundation of China (No. 50973105 and No. 50773078), the CAS Knowledge Innovation Program (No. KGCX2-YW-326), the Key Scientific and Technological Program of Jilin Province (No. 10ZDGG012), and the CAS Hundred Talent Program are acknowledged for financial support. We are grateful to Dyesol for supplying the WERO-2 scattering paste and EMITCB, and to DuPont Packaging and Industrial Polymers for supplying the Bynel film.

References and Notes

(1) O'Regan, B.; Grätzel, M. *Nature* **1991**, *353*, 737–740.
(2) Grätzel, M. *Acc. Chem. Res.* **2009**, *42*, 1788–1798.
(3) Chiba, Y.; Islam, A.; Watanabe, Y.; Komiya, R.; Koide, N.; Han, L. *Jpn. J. Appl. Phys. Part 2* **2006**, *45*, L638–L640.
(4) Hara, K.; Kurashige, M.; Dan-oh, Y.; Kasada, C.; Shinpo, A.; Suga, S.; Sayama, K.; Arakawa, H. *New J. Chem.* **2003**, *27*, 783–785.
(5) Kitamura, T.; Ikeda, M.; Shigaki, K.; Inoue, T.; Anderson, N. A.; Ai, X.; Lian, T.; Yanagida, S. *Chem. Mater.* **2004**, *16*, 1806–1812.
(6) Justin Thomas, K. R.; Lin, J.-T.; Hsu, Y.-C.; Ho, K.-C. *Chem. Commun.* **2005**, 4098–4100.
(7) Koumura, N.; Wang, Z.-S.; Mori, S.; Miyashita, M.; Suzuki, E.; Hara, K. *J. Am. Chem. Soc.* **2006**, *128*, 14256–14257.
(8) Horiuchi, T.; Miura, H.; Sumioka, K.; Uchida, S. *J. Am. Chem. Soc.* **2004**, *126*, 12218–12219.
(9) Mishra, A.; Fischer, M. K. R.; Bäuerle, P. *Angew. Chem., Int. Ed.* **2009**, *48*, 2474–2499.
(10) Gorlov, M.; Kloo, L. *Dalton Trans.* **2008**, 2655–2666.

(11) Zakeeruddin, S. M.; Grätzel, M. *Adv. Funct. Mater.* **2009**, *9*, 2187–2202.
(12) Kubo, W.; Kitamura, T.; Hanabusa, K.; Wada, Y.; Yanagida, S. *Chem. Commun.* **2002**, 374–375.
(13) MacFarlane, D. R.; Forsyth, M.; Howlett, P. C.; Pringle, J. M.; Sun, J.; Annat, G.; Neil, W.; Izgorodina, E. I. *Acc. Chem. Res.* **2007**, *40*, 1165–1173.
(14) Bai, Y.; Cao, Y.; Zhang, J.; Wang, M.; Li, R.; Wang, P.; Zakeeruddin, S. M.; Grätzel, M. *Nat. Mater.* **2008**, *7*, 626–630.
(15) Kuang, D.; Wang, P.; Ito, S.; Zakeeruddin, S. M.; Grätzel, M. *J. Am. Chem. Soc.* **2006**, *128*, 7732–7733.
(16) MacFarlane, D. R.; Golding, J.; Forsyth, S.; Forsyth, M.; Deacon, G. B. *Chem. Commun.* **2001**, 1430–1431.
(17) Haque, S. A.; Tachibana, Y.; Klug, D. R.; Durrant, J. R. *J. Phys. Chem. B* **1998**, *102*, 1745–1749.
(18) Haque, S. A.; Tachibana, Y.; Willis, R. L.; Moser, J.-E.; Grätzel, M.; Klug, D. R.; Durrant, J. R. *J. Phys. Chem. B* **2000**, *104*, 538–547.
(19) Pelet, S.; Moser, J.-E.; Grätzel, M. *J. Phys. Chem. B* **2000**, *104*, 1791–1795.
(20) Ardo, S.; Meyer, G. J. *Chem. Soc. Rev.* **2009**, *38*, 115–164.
(21) Koops, S. E.; O'Regan, B. C.; Barnes, P. R. F.; Durrant, J. R. *J. Am. Chem. Soc.* **2009**, *131*, 4808–4818.
(22) O'Regan, B. C.; Durrant, J. R. *Acc. Chem. Res.* **2009**, *42*, 1799–1808.
(23) Fabregat-Santiago, F.; Bisquert, J.; Garcia-Belmonte, G.; Boschloo, G.; Hagfeldt, A. *Sol. Energy Mater. Sol. Cells* **2005**, *87*, 117–131.
(24) Bisquert, J. *J. Phys. Chem. B* **2002**, *106*, 325–333.
(25) Fabregat-Santiago, F.; Garcia-Belmonte, G.; Bisquert, J.; Zaban, A.; Salvador, P. *J. Phys. Chem. B* **2002**, *106*, 334–339.
(26) Bisquert, J.; Grätzel, M.; Wang, Q.; Fabregat-Santiago, F. *J. Phys. Chem. B.* **2006**, *110*, 11284–11290.
(27) Rühle, S.; Greenshtein, M.; Chen, S.-G.; Merson, A.; Pizem, H.; Sukenik, C. S.; Cahen, D.; Zaban, A. *J. Phys. Chem. B* **2005**, *109*, 18907–18913.
(28) Bisquert, J. *Phys. Chem. Chem. Phys.* **2003**, *5*, 5360–5365.
(29) Koelsch, M.; Cassaignon, S.; Ta Thanh Minh, C.; Guillemoles, J.-F.; Jolivet, J.-P. *Thin Solid Films* **2004**, *451−452*, 86–92.
(30) Barea, E. M.; Zafer, C.; Gultekin, B.; Aydin, B.; Koyuncu, S.; Icli, S.; Fabregat-Santiago, F.; Bisquert, J. *J. Phys. Chem. C* **2010**, *114*, 19840–19848.
(31) Bisquert, J.; Mora-Seró, I. *J. Phys. Chem. Lett.* **2010**, *1*, 450–456.
(32) Potscavage, W. J., Jr.; Sharma, A.; Kippelen, B. *Acc. Chem. Res.* **2009**, *42*, 1758–1767.
(33) Bonhôte, P.; Dial, A. P.; Papageorgiou, N.; Kalyanasumdaram, K.; Grätzel, M. *Inorg. Chem.* **1996**, *35*, 1168–1178.
(34) Li, R.; Liu, J.; Cai, N.; Zhang, M.; Wang, P. *J. Phys. Chem. B* **2010**, *114*, 4461–4464.
(35) Wang, P.; Zakeeruddin, S. M.; Comte, P.; Charvet, R.; Humphry-Baker, R.; Grätzel, M. *J. Phys. Chem. B* **2003**, *107*, 14336–14341.
(36) Runge, E.; Gross, E. K. U. *Phys. Rev. Lett.* **1984**, *52*, 997–1000.
(37) Becke, A. D. *J. Chem. Phys.* **1993**, *98*, 5648–5652.
(38) Lee, C.; Yang, W.; Parr, R. G. *Phys. Rev. B.* **1988**, *37*, 785–789.
(39) Frisch, M. J.; Trucks, G. W.; Schlegel, H. B.; Scuseria, G. E.; Robb, M. A.; Cheeseman, J. R. ; Montgomery, J. A., Jr.; Vreven, T.; Kudin, K. N.; Burant, J. C.; Millam, J. M.; Iyengar, S. S.; Tomasi, J.; Barone, V.; Mennucci, B.; Cossi, M.; Scalmani, G.; Rega, N.; Petersson, G. A.; Nakatsuji, H.; Hada, M.; Ehara, M.; Toyota, K.; Fukuda, R.; Hasegawa, J.; Ishida, M.; Nakajima, T.; Honda, Y.; Kitao, O.; Nakai, H.; Klene, M.; Li, X.; Knox, J. E.; Hratchian, H. P.; Cross, J. B.; Bakken, V.; Adamo, C.; Jaramillo, J.; Gomperts, R.; Stratmann, R. E.; Yazyev, O.; Austin, A. J.; Cammi, R.; Pomelli, C.; Ochterski, J. W.; Ayala, P. Y.; Morokuma, K.; Voth, G. A.; Salvador, P.; Dannenberg, J. J.; Zakrzewski, V. G.; Dapprich, S.; Daniels, A. D.; Strain, M. C.; Farkas, O.; Malick, D. K.; Rabuck, A. D.; Raghavachari, K.; Foresman, J. B.; Ortiz, J. V.; Cui, Q.; Baboul, A. G.; Clifford, S.; Cioslowski, J.; Stefanov, B. B.; Liu, G.; Liashenko, A.; Piskorz, P.; Komaromi, I.; Martin, R. L.; Fox, D. J.; Keith, T.; Al.Laham, M. A.; Peng, C. Y.; Nanayakkara, A.; Challacombe, M.; Gill, P. M. W.; Johnson, B.; Chen, W.; Wong, M. W.; Gonzalez, C.; Pople, J. A. *Gaussian 09*, revision A.02; Gaussian Inc.: Wallingford CT, 2009.

JP109803N